Electrochemical detection of a single cytomegalovirus at an ultramicroelectrode and its antibody anchoring

Jeffrey E. Dick[a], Adam T. Hilterbrand[b], Aliaksei Boika[a,1], Jason W. Upton[b], and Allen J. Bard[a,2]

[a]Department of Chemistry, Center for Electrochemistry, The University of Texas at Austin, Austin, TX 78712; and [b]Department of Molecular Biosciences, Institute for Cellular and Molecular Biology, The University of Texas at Austin, Austin, TX 78712

Contributed by Allen J. Bard, March 12, 2015 (sent for review February 1, 2015; reviewed by Rebecca Lai and Nat Moorman)

We report observations of stochastic collisions of murine cytomegalovirus (MCMV) on ultramicroelectrodes (UMEs), extending the observation of discrete collision events on UMEs to biologically relevant analytes. Adsorption of an antibody specific for a virion surface glycoprotein allowed differentiation of MCMV from MCMV bound by antibody from the collision frequency decrease and current magnitudes in the electrochemical collision experiments, which shows the efficacy of the method to size viral samples. To add selectivity to the technique, interactions between MCMV, a glycoprotein-specific primary antibody to MCMV, and polystyrene bead "anchors," which were functionalized with a secondary antibody specific to the Fc region of the primary antibody, were used to affect virus mobility. Bead aggregation was observed, and the extent of aggregation was measured using the electrochemical collision technique. Scanning electron microscopy and optical microscopy further supported aggregate shape and extent of aggregation with and without MCMV. This work extends the field of collisions to biologically relevant antigens and provides a novel foundation upon which qualitative sensor technology might be built for selective detection of viruses and other biologically relevant analytes.

collisions | cytomegalovirus | electrochemistry | murine cytomegalovirus | virus

Over the past decade, the study of discrete collision events on ultramicroelectrodes (UMEs) has gained attention due to the interest in understanding stochastic phenomena by electrochemistry. By observing the collisions of small particles, there is the possibility that information can be deduced that is not available in ensemble measurements. The electrochemical study of single collision events has been applied to a wide range of hard nanoparticles (NPs), which include metal, metal oxide, and organic NPs [platinum (1), silver (2), gold (3), nickel (4), copper (5), iridium oxide (6), cerium oxide (7), titanium oxide (8), silicon oxide (9), indigo (10), polystyrene (11), and relatively large aggregates of fullerene (12)]. Recently, collisions of soft particles have been investigated, such as toluene droplets (13) and liposomes (14). Also, collisions of toluene and tri-*n*-propylamine droplets were observed simultaneously by both electrochemical and electrogenerated chemiluminescent (ECL) measurements (15).

Similarly, a variety of techniques have been developed to observe these collision events. The interested reader can consult the references for a discussion on each of the techniques used to observe stochastic events electrochemically: blocking (9, 13), electrocatalytic amplification (1), open circuit potential (16), droplet blocking/reactor (13, 14), and ECL (15, 17,18). The simplest and most reproducible method of observing collisions is a technique termed blocking, which is so named because particles, which are brought to the electrode by a diffusion-limited flux and/or electrophoretic migration, irreversibly adsorb (1) to the electrode surface, blocking the flux of redox active species. In this experiment, an appropriate concentration of redox active species is dissolved into the aqueous continuous phase such that individual adsorption events can be distinguished from the background. Potassium ferrocyanide [$K_4Fe(CN)_6$, KFCN, E^o = ~0.24 V vs. Ag/AgCl], was chosen as the redox active species in this study because KFCN incompletely dissociates during dissolution (19–21) due to ion pairing (22). This incomplete dissociation is advantageous in solutions of colloidal suspensions because high ionic strength media will cause suspensions to aggregate. This means that solutions of 100–400 mM KFCN are achievable without noticeable aggregation of particles over the time scale of the experiments, which has been observed for less stable (zeta, ζ-potential = −15 mV) toluene droplets in 200 mM KFCN (13). When an insulating particle, suspended in the aqueous solution of KFCN, stochastically collides with the UME surface, it blocks the flux of redox active species, which manifests itself as a current step in amperometry. The cause of this step shape is an almost instantaneous decrease in steady-state current upon collision of the particle with the electrode surface followed by a leveling off at a new steady-state current value.

Because of the success in studying many systems using collisions, such as early work using electrocatalytic amplification as a sensitive means of detecting DNA (23), it was our hope to extend the field of collisions to more biologically relevant species, such as viruses. Cytomegaloviruses (CMVs) are the prototypic members of the β-herpesvirus family. These large (100–200-nm) dsDNA viruses establish lifelong latent infections after primary infection and do not cause significant disease in healthy individuals. However, immunocompromised individuals infected with human cytomegalovirus (HCMV) are at a significantly greater risk of morbidity and mortality (24), including patients receiving chemotherapeutics, AIDS patients, and organ transplant recipients. Moreover, HCMV congenital infection is a leading cause of birth defects and developmental disabilities including hearing and vision loss, microcephaly, and cognitive disabilities (25). Thus, highly sensitive and rapid detection of CMV infection in patients is an important part of mitigating transmission and disease. Like most herpesviruses,

Significance

The need for rapid, dependable, and sensitive detection of biological threats is ever increasing. Relatively arduous techniques, with varying degrees of sensitivity, exist for the detection of pathogens, including ELISA, electrogenerated chemiluminescence methods, sensitive PCR techniques, culturing, and microscopy. Here, we extend the observation of particle collisions on ultramicroelectrodes to murine cytomegalovirus. We further present an electrochemical technique for the specific detection of low concentrations of a virus by observing the effect of virus and antibody-specific polystyrene bead binding. This work, in principle, provides a framework for the detection of any biologically relevant antigen.

Author contributions: J.E.D. and A.J.B. designed research; J.E.D., A.T.H., A.B., and J.W.U. performed research; J.E.D., A.T.H., A.B., J.W.U., and A.J.B. analyzed data; and J.E.D., A.T.H., A.B., J.W.U., and A.J.B. wrote the paper.

Reviewers: R.L., University of Nebraska-Lincoln; and N.M., University of North Carolina at Chapel Hill.

The authors declare no conflict of interest.

[1]Present address: Department of Chemistry, The University of Akron, Akron, OH 44325.

[2]To whom correspondence should be addressed. Email: ajbard@mail.utexas.edu.

This article contains supporting information online at www.pnas.org/lookup/suppl/doi:10.1073/pnas.1504294112/-/DCSupplemental.

HCMV is highly species specific, and murine cytomegalovirus (MCMV) serves as an important model system for HCMV pathogenesis, sharing significant genetic and biological characteristics. MCMV provides a powerful, genetically tractable infection system in a natural mouse host and has yielded significant insights into CMV biology. Relatively arduous techniques, with varying degrees of sensitivity, exist for the detection of pathogens, including ELISA methods, sensitive PCR techniques, culturing, ECL, and microscopy. A comparison of these techniques with the proposed electrochemical technique is given in *SI Appendix*.

In this article, the electrochemical study of discrete collision events is extended to the detection of biological species. Due to the widespread interest in rapid diagnostics for infectious diseases, quick and sensitive techniques to detect ultralow concentrations of biologically relevant species are actively being investigated across many fields of research. Detection of dilute concentrations of pathogens is an especially important goal. The utilization of electrochemical collisions has been demonstrated to be sensitive enough to differentiate nanoparticle aggregates, such as aggregates of silver nanoparticles from monomers and dimers to higher order aggregates (26). Here, we present a technique to selectively detect viruses based on blocking and specific interactions between MCMV, an MCMV-specific antibody, and polystyrene beads (PSBs). The viruses act as a type of "bond" between the PSBs and cause aggregation, which manifests itself in two ways during a collision experiment: a decrease in frequency of collision, due to an overall decrease in diffusion coefficient of the aggregates versus single beads, and larger current step heights, due to rare collisions of larger aggregates.

Electrochemical Detection of Discrete CMV Collisions

Fig. 1*A* is a representation of CMV. Fig. 1*B* gives a representation of the blocking experiment in KFCN. An aqueous solution of KFCN was prepared by dissolving 500 mM KFCN into a volume of water. When the potential of an UME is held at the mass transfer limited current (~+0.4 V vs. Ag/AgCl for KFCN), as shown by the steady-state current value achieved in cyclic voltammetry (*SI Appendix*, Fig. S1), single collision events of MCMV can be observed, as evidenced by the two current steps in the chronoamperogram in Fig. 1*B*. A collision event is marked by a rapid decrease in current, followed by a leveling off to a lower steady-state current value. Fig. 1*B* displays a chronoamperogram on a 10-μm Pt UME. Here, ~0.86 pM of virus (5.2×10^5 viruses per microliter) was in a solution of KFCN. The adsorption of the virus to the electrode surface causes the current steps. Because no electrolyte was added in the experiment represented in Fig. 1*B*, electrophoretic migration to the electrode surface is likely the dominant mode of mass transport along with diffusion (9), vide infra.

Experiments with the virus alone were carried out, as described above. The study of blocking collisions gives insight into two observable parameters within the current response. First, the current step size gives an estimate of the footprint of the colliding particle on the electrode surface. Because the current density is highest at the edges of the circular disk-shaped electrode because of radial mass transport (27), an adsorption event at the edge of the electrode will block a larger flux than a collision event that occurs at the center of the electrode. Because of this edge effect, a distribution of current step heights is obtained (see Fig. 3). Second, the frequency of collision can be calculated theoretically by assuming a diffusion-limited flux of particles to the electrode surface and experimentally by counting the number of collision events over time. The frequency of collision based on diffusion (28), $f_{D,\ theoretical}$, is given by

$$f_{D,\mathrm{theoretical}} = 4\mathrm{DCr_eN_A}, \qquad [1]$$

where N_A is Avogadro's number, r_e is the radius of the electrode, C is the concentration of colloid in solution, and D is the diffusion coefficient of the particular particle. The concentrations of the

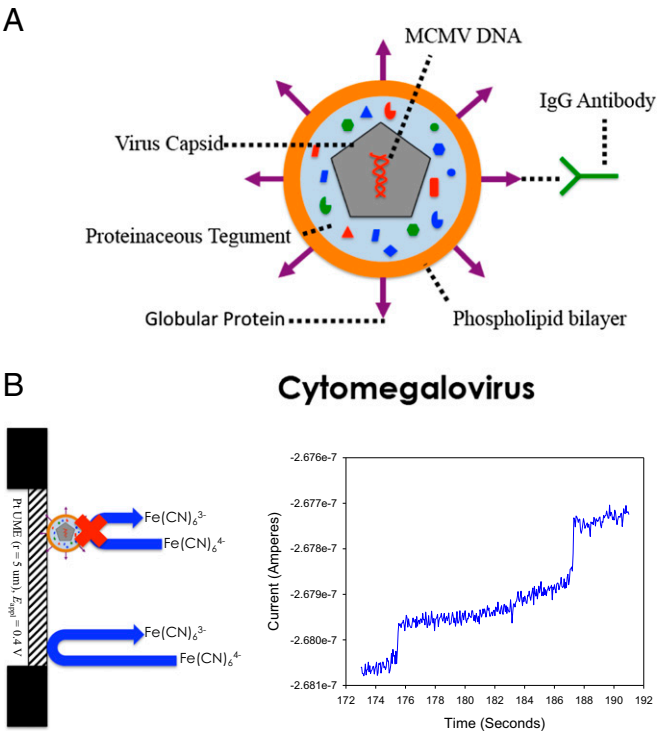

Fig. 1. (*A*) Schematic representation of a CMV virion. The antibody used in these studies is specific for the gB protruding from the phospholipid bilayer surface. (*B*) Typical blocking response. Steps in the *i*–*t* curve represent individual adsorption events of MCMV onto the electrode surface. MCMV is blocking 500 mM KFCN at a 10-μm Pt UME, where E_{appl} = +0.4 V vs. Ag/AgCl.

MCMV and MHV-68 (a virus used for negative control in gaining specificity with the primary antibody) were determined using nanoparticle tracking analysis (NTA), which tracks individual particles and determines a size distribution based on the diffusion coefficient using the random walk model. The hydrodynamic radius of the assumed spherical particle can be calculated from the Stokes–Einstein relation (29):

$$\mathrm{r_{particle}} = \mathrm{k_BT}(6\pi\eta\mathrm{D})^{-1}, \qquad [2]$$

where $r_{particle}$ is the radius of the particle, k_B is Boltzmann's constant, T is temperature, and η is the viscosity of the continuous phase.

Electrochemical Detection of CMV with CMV-Specific Antibody

Herpesviruses, such as MCMV, are enveloped viruses with surface glycoproteins protruding from the surface of the phospholipid bilayer (Fig. 1*A*). Glycoprotein B (gB), one of the major envelope glycoproteins in herpesviruses, functions to facilitate attachment to host cell receptors and mediate fusion of the viral envelope with the host cell membrane (30). MAb 97.3 is a neutralizing monoclonal antibody raised against MCMV gB and is effective at preventing MCMV infection in vitro and in vivo (31). The ζ-potential of MCMV, as measured by NTA with a Nanosight instrument, is −35 mV in 10 mM PBS, suggesting that MCMV is negatively charged and stable. The ζ-potential of MCMV with antibody (MCMV-Ab) was −32 mV. NTA was also used to show that the average hydrodynamic radius of the virus increased upon addition of antibody (*SI Appendix*). Using the electrochemical collision technique, we show similar results by looking at differences in current step size and step frequency between MCMV and MCMV-Ab.

Table 1 contains the average values of the current steps measured for more than 500 collision events for MCMV and MCMV-Ab.

Table 1. Statistics of MCMV and MCMV-A, values of diffusion coefficient and radii

Sample	Number of events	ΔI(pA)	δ	f, Hz	δ	D, cm^2/s	D, cm^2/s*	R, nm
MCMV	523	224	17	0.046	0.006	4.4×10^{-8}	6.4×10^{-8}	56
MCMV-Ab	506	293	21	0.034	0.008	3.3×10^{-8}	3.6×10^{-8}	73

*Values from NTA.

Also shown are values of frequency, calculated over the same number of events. From the frequency data tabulated by counting discrete events using collisions on an UME, D is calculated and compared with NTA. The values of $r_{particle}$ are then calculated from the Stokes–Einstein relation.

According to the results in Table 1, the diffusion coefficients calculated electrochemically are in good agreement with D calculated using NTA. By measuring the current step height, we can get an idea of the concentration of KFCN that MCMV-Ab will block relative to MCMV alone. This simple ratio is calculated by taking the ratio of the amount of current blocked at the electrode surface, or 293/224 = 1.31. Assuming that the amount of redox active species that is blocked is proportional to the maximum cross-sectional surface area of the particle blocking (i.e., the "footprint"), the predicted ratio is $73^2/56^2 = 1.70$. The discrepancy that results between the current step ratio and the ratio of the radii may result from the edge effect (species are landing at different locations on the electrode surface) and because the entire hemispherical area does not block the electrode surface (Fig. 1). Interestingly, the difference between the radius of MCMV-Ab and MCMV is 17 nm, based on the electrochemical data (see *Discussion* for more details). This value agrees remarkably well with the reported length of the IgG antibody in the literature of 14.5 nm (32). This surprising result implies that electrochemical collision events may be sensitive enough to resolve the difference of 17 nm in hydrodynamic radius.

Selectivity by Antibody Anchoring of PSBs

In addition to tracking single collisions of viruses, it is desirable to have some means of identifying the virus through collisions. To help identify the viruses in collision experiments, we showed the effect of virus on collisions of 750-nm PSBs whose surface was functionalized with a secondary antibody that will specifically bind to the Fc region of the primary antibody to MCMV. Here, a specific aggregation or "anchoring" approach, where the interaction of the virus with the 750-nm PSBs greatly decreased the mobility of the PSBs, effectively removes PSBs as a colliding species. Letsinger and coworkers, who observed the color change of a gold colloidal system when the gold NPs were functionalized with cDNA oligomers, have used this anchoring approach as an ensemble technique (33, 34). Fig. 2 gives an illustration of the experiment. Here, the PSBs are functionalized with a secondary antibody that will specifically bind to the primary antibody. As shown in Fig. 2*A*, the presence of both virus and its antibody will facilitate aggregation of the PSBs. In this experiment, the concentration of redox-active species in the continuous phase is held at 100 mM, such that the stochastic collisions of individual viruses are indiscernible from the background. This allows for the direct observation of PSBs and the effect that the virus has on the beads without having to deconvolute the collisions of two different species. Fig. 2*B* shows an illustration of the electrochemical response for the assay without virus and the assay with virus. Because the virus facilitates aggregation, a lack of virus will result in collisions of PSBs. Upon addition of the virus, aggregation of the PSBs will occur. Therefore, the virus is acting as a type of bond between different beads (*SI Appendix*, Fig. S2). Because the aggregates are larger than the monomeric PSBs, the average diffusion coefficient will decrease, which will decrease the frequency of collisions. However, if an aggregate does collide with the electrode, a large current step will be observed, several times larger than the average current step of the PSB alone and much larger than the response of a single virus. If the primary antibody is not specific to the analyte of interest, no aggregates will form over the course of the

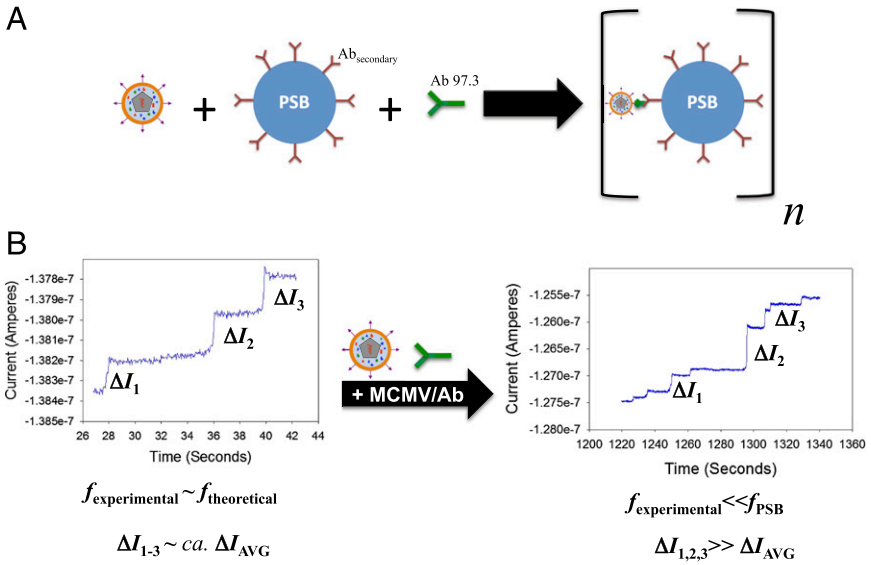

Fig. 2. (*A*) Schematic representation of the collision experiments with PSBs radius, 750 nm, binding to the virus through the primary antibody (green Y). The secondary antibodies (maroon Ys) are specific to the Fc region of the primary antibody. (*B*) Electrochemical current responses with and without virus. Without the virus, collisions of PSBs are observable with a characteristic frequency and current step height, ΔI. Upon addition of virus, the frequency drops, relative to the frequency of PSBs alone, and larger current steps can be observed.

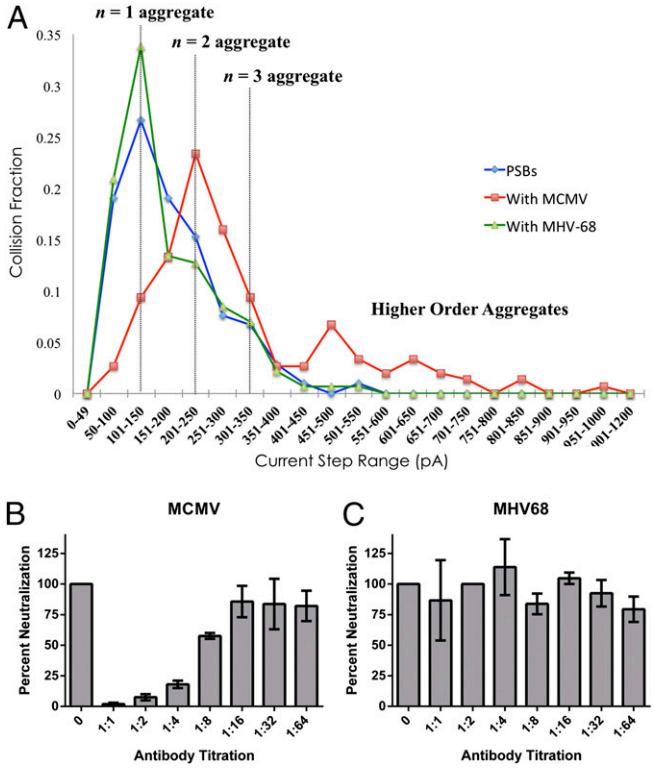

Fig. 3. (*A*) Current step distributions of the amount of collisions counted (collision fraction) as a function of current step binning. PSBs and virus are in a 1:1 mol ratio. Current step size distributions were determined for PSB and MAb 97.3 (blue trace), PSB and MAb 97.3 with MCMV (red trace), and PSB and MAb 97.3 with MHV68 (green trace). Aggregates of $n = 1$, 2, 3 and higher order were counted using amperometry of 100 mM KFCN dissolved in the aqueous continuous phase on a 10-μm Pt UME. The potential was held at +0.4 V vs. Ag/AgCl. (*B* and *C*) Plaque reduction neutralization tests for MCMV and MHV68 with MAb 97.3 (see text).

experiment, and no difference in the electrochemical response is observed. Experiments were carried out with 1:1, 2:1, 5:1, and 10:1 PSB to virus mole ratio. No significant change in frequency or step size was observed for collision experiments with 5:1 and 10:1 mol ratio.

Fig. 3 represents the current step distribution for the PSBs (blue trace) and PSBs with MCMV (red trace). Addition of MCMV causes aggregation (difference between blue and red traces), which is shown in the shift of the distribution to larger current step sizes. This shift implies that the virus causes the aggregation to occur, favoring higher order aggregates. To demonstrate specificity, control experiments were conducted with another herpesvirus, murine γ-herpesvirus-68 (MHV68). MHV68 has a ζ-potential of −29 mV and a size distribution centering around 200 nm under the same conditions (see *SI Appendix* for more NTA details). The green trace shows no shift from the blue PSB distribution (Fig. 3*A*), suggesting the primary antibody fails to bind MHV68. To verify the efficacy and specificity of the neutralization antibody (M 97.3), plaque reduction neutralization tests were performed. Increasingly dilute concentrations of MAb 97.3 were incubated with a constant concentration of MCMV or MHV-68, and assessed for infectivity by plaque assay. MCMV infectivity was significantly diminished by increasing concentrations of MAb 97.3 (Fig. 3*B*), whereas MHV68 infectivity remained unaffected (Fig. 3*C*), demonstrating the specificity of MAb 97.3 directly correlates with the ability of MCMV to induce the observed PSB aggregates (Fig. 3*A*). The decrease in infectivity is due to the binding of MAb 97.3, which binds to the gB protein on the surface of MCMV. Because the gB protein is responsible for the fusion of the virus with the mammalian cell membrane, by blocking this protein, the virus cannot infect the cell.

Analysis of Bead Aggregates by Microscopy

A careful analysis of the distribution shape shows three specific peaks in the polystyrene background, which are believed to be aggregates with $n = 1$, 2, 3. To probe the various shapes, dynamic light scattering (DLS) was used (*SI Appendix*), as well as optical microscopy and scanning electron microscopy (SEM). Fig. 4 shows both optical and SEM images of the different types of shapes of PSBs in the presence of virus. Without virus, the beads are largely monodisperse, and no higher order aggregates are observed (*SI Appendix*, Fig. S3). SEM was used to observe the shapes; however, because this technique requires evaporation of solvent and is sensitive to evaporation rate and concentration, optical microscopy was used to confirm the shapes observed in SEM and electrochemistry. Fig. 4 *F*–*J* provides evidence by an optical image of several types of aggregates of beads in the presence of virus on the coverslip. The addition of virus caused more aggregation, and unique shapes, such as the $n = 6$ presented in Fig. 4, were also observed optically along with much larger aggregates (Fig. 4 and *SI Appendix*, Fig. S4).

Effect of Electrophoretic Migration

Because the mass transport of viruses or PSBs (charged colloids) to the electrode surface is the sum of the diffusional and migrational fluxes (35), a comparison of frequency with and without supporting electrolyte can be used to estimate the electrophoretic migration contribution to mass transport of analyte species. To achieve this, experiments were performed with and without 50 mM KNO_3 as a supporting electrolyte. We assumed that the addition of 50 mM KNO_3 would decrease the contribution of migration to the overall flux of the analyte species. This is so because the potassium and nitrate ions participate in the transfer of ionic charge thus decreasing the contribution of viruses or PSB to the total current. Table 2 shows the results of these experiments. The migrational component to flux for the virus was expected to be low because the value of diffusion coefficient calculated electrochemically was similar to the value calculated using NTA. An empirical relationship for diffusional flux, described in *Discussion*, allowed the calculation of the theoretical frequency of the species colliding with the UME, shown in Table 2 ($f_{D,\ theoretical}$). One can see that in the case of PSBs, the frequency of collisions is much larger than what is expected for the transfer of the analyte species by diffusion only; this suggests the presence of migration as the dominant mode of mass transfer of the species. Moreover, the addition of 50 mM KNO_3 decreased the frequency of observed collisions, which can be explained by the decrease of the contribution of migration to the total flux of PSB. This is in agreement with the previously published data (9, 34). However, the addition of 50 mM KNO_3 did not have an effect on the frequency of collisions of virus particles. This means that the virus is transferred by diffusion, which agrees with $f_{D,\ no\ KNO3} \sim f_{D,\ theoretical}$. The exact reasons for the observed effect are not clear to us, and further investigation is required.

Note that migration can be used as an advantageous preconcentration tool, which potentially makes possible the detection of femto- to attomolar concentrations. Currently, most electrochemical immunoassay systems use magnetic beads as the preconcentration technique for collisions (36) and ECL (37). The use of electrophoretic migration provides a more general technique based on the charge of the particles and the electrical field supplied by the electrodes in solution.

Table 2. Effect of additional electrolyte to collision frequency

Species	[KFCN]	$f_{experimental}$	f_{KNO3}	Migration contribution, %
Virus	400	0.046	0.044	4
PSB	100	0.071	0.008	89

Concentration of virus and PSB was held at 0.283 pM, and the concentration of KNO_3 was held at 50 mM.

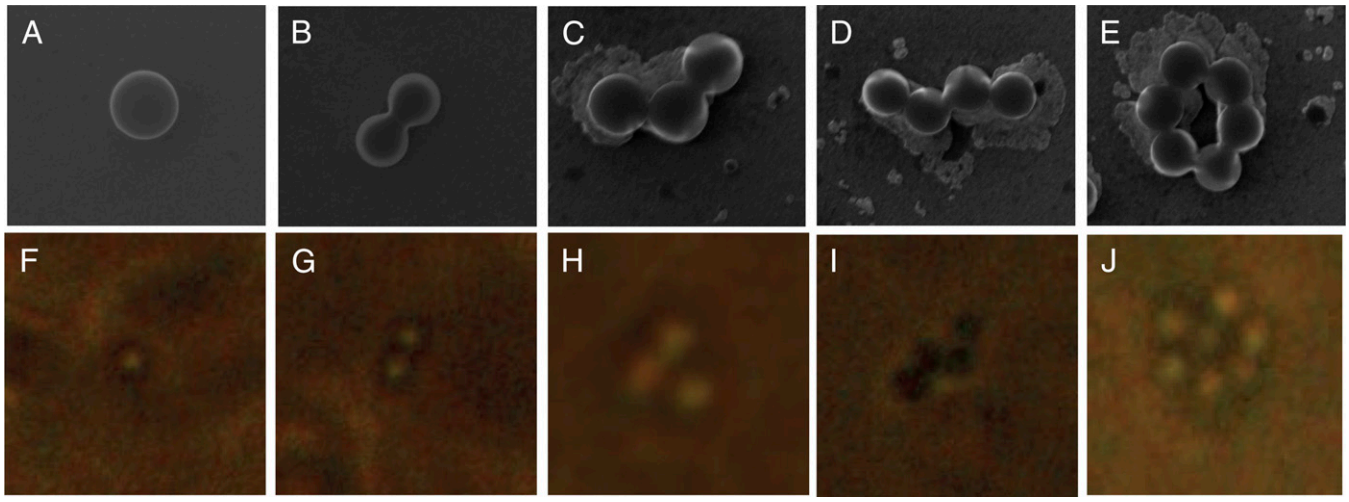

Fig. 4. (*A–E*) Scanning electron micrographs of 0.283-pM PSBs and virus (1:1 stoichiometry), examples of n = 1, 2, 3, 4, ... aggregates and their optical microscope analogs (*F–J*) taken with a 100× objective lens. In each case, the diameter of the bead was measured to be 750 nm.

Discussion

Whereas stochastic collisions of the virus alone are observable using the electrochemical technique, the method based on addition of PSBs to the system allowed for specific detection of a β-herpesvirus, MCMV, using the electrochemical collision technique. By using MHV68, a γ-herpesvirus that the antibody would not neutralize (i.e., prevent its infectiousness), we demonstrate the specificity of the demonstrated technique. Upon addition of the virus selective to the primary antibody in our assay (MCMV recognized by MAb 97.3), a clear shift in current step distribution is observed. This change in current step distribution can be coupled to a change in frequency of collision, further demonstrating the diagnostic nature of this approach. Fig. 5 shows a plot of collision frequency versus concentration for a system with 15:1 MCMV-A to PSB. The frequency of collisions decreases by over 80% when there is an excess of virus compared with PSB. By tracking the changes in frequency and current step height, a qualitative diagnosis can be made. Research into quantitative determinations of biologically relevant antigens using the proposed collision technique is being actively pursued.

In summary, we have extended the field of collisions on UMEs to biologically relevant antigens, i.e., viruses. We have also presented an electroanalytical technique for the qualitative and specific measure of MCMV based on collisions on UMEs. This was achieved by monitoring the collisions of a reference particle, a PSB, which is functionalized with a secondary antibody that will bind to the primary antibody. In the presence of virus, this binding interaction will cause the PSBs to aggregate. By monitoring the frequency of collision and the current step height during chronoamperometry, the extent of this aggregation can be qualitatively determined and give insight into whether or not virus is present in the sample. This work, in principle, provides a framework for the detection of any biologically relevant antigen, and we are investigating other antigen and DNA systems. This work also potentially provides a means of observing the specificity of a particular antibody. Many factors can be changed to increase the sensitivity of this technique, such as the electrolyte concentration can change to affect electrophoretic migration, the stoichiometric ratio of virus to PSB can also be optimized, and the concentration can then be pushed down to a limit such as to see a recordable frequency in a feasible amount of time. The application of other collision techniques, such as electrocatalytic amplification, is being actively pursued as another means of specifically detecting antigens, other than DNA, and by monitoring stochastic collisions electrochemically. We believe that this work provides a novel foundation upon which sensor technology for various analytes of interest can be evolved from this electrochemical collision technique.

Materials and Methods

Chemicals. Water used in each experiment was Milli-Q water. Ferrocyanide was purchased from Fisher Scientific and used without further purification. Ferrocenedimethanol was purchased and used without further purification. Goat anti-mouse IgG (Fc) coated polystyrene particles (0.7–0.9 μm) were purchased from Spherotech and stored at 4 degrees centigrade. Before using the solution, the bottle was vortexed for 1 min and sonicated using a Q500 ultrasonic processor (Qsonica). Potassium nitrate (KNO_3, 99.8%) was purchased from Fisher Scientific. All chemicals were used as received.

Electrochemistry. Electrochemical experiments were performed using a CHI model 900B potentiostat (CH Instruments). The Pt UME was prepared following the general procedure developed in our laboratory (38). The three-electrode cell was placed in a faraday cage and grounded to a pipe. A Ag/AgCl (1 M KCl) wire was used (BASi) as the reference electrode, and a Pt wire was used as the auxiliary electrode. Generally, experiments were performed in a 20-mL glass vial with a homemade vial cap to position the electrodes in the solution.

Optical Analysis. DLS was obtained using a Zetasizer Nano ZS (Malvern). NTA was also used to analyze the virus particles by Nanosight. Here, scattering light from a laser illuminates particles. A movie of these particles is taken, and the software traces the movement of the nanoparticle. This movement allows the software to calculate a diffusion coefficient and use the Stokes–Einstein

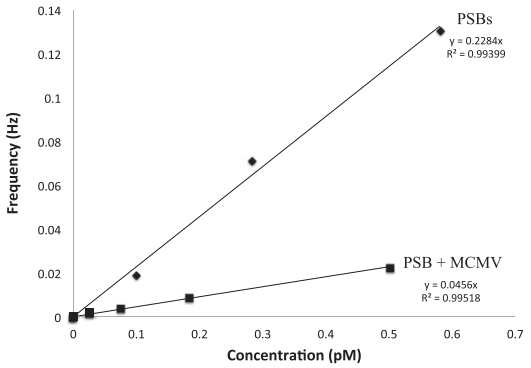

Fig. 5. Frequency versus concentration for PSBs and PSBs with excess MCMV. Collisions were counted in amperometry of 100 mM KFCN dissolved in the aqueous continuous phase on a 10-μm Pt UME. The potential was held at +0.5 V vs. Ag/AgCl.

relation to back-calculate the hydrodynamic radius. SEM images were obtained using an FEI Quanta 650 ESEM. The optical images were taken using a Nikon Eclipse TE300 inverted microscope with a 100× objective lens and a camera attachment to the eyepiece.

Virus Propagation and Purification. Bacterial artificial chromosome derived wild-type MCMV (strain K181-Perth) and MHV68 WUMS [obtained from American Type Culture Collection (ATCC) #VR1465] were generated on NIH 3T3 fibroblasts (ATCC, #CRL-1658) as previously described (39, 40). Viral stocks were propagated, clarified, and concentrated as previously described (41). Sorbitol density gradient purification was performed as previously described to purify the virus (42). Briefly, concentrated virus was resuspended in complete DMEM supplemented with 10% bovine calf serum, layered over 20% sucrose cushion, and centrifuged 60 min at 32,800 × *g*. Pelleted virus was resuspended in Tris-buffered saline (0.05 M Tris, 0.10 M NaCl, pH 7.4), placed onto a 20–70% continuous linear sorbitol gradient, and subjected to ultracentrifugation at 70,000 × *g* for 60 min at 16 °C. Virion band was visualized using light scatter from an overhead light source, and collected by needle aspiration. Samples were subjected to a second round of ultracentrifugation to remove additional contaminants.

Antibody and Bead Adsorption. Mouse monoclonal anti-gB neutralizing antibody (Clone MAb97.3) was provided by Michael Mach, University of Erlangen, Germany. Preparation of the MCMV-A samples was as follows: Infectivity experiments were completed to gauge how much antibody would render the virus noninfectious under the assumption that a noninfectious virus is saturated with antibody. Details of this experiment are provided in *SI Appendix*. A 1:1 (vol/vol) virus to antibody solution was mixed together and allowed to incubate at 37 degrees centigrade for 1 h in warm water. A new sample was made for each experiment, and experiments were performed in triplicate. For the MHV68, a similar method of preparation was performed as for MCMV. For the PSB measurements, a similar procedure was followed. Here, the PSBs were added to the virus and antibody mixture. The PSB, MCMV, Ab 97.3 mixture was incubated at room temperature for another hour.

ACKNOWLEDGMENTS. The authors thank Dr. Michael Mach for the donation of mouse monoclonal anti-gB neutralizing antibody (MAb 97.3). J.E.D. and A.B. thank Dr. Christophe Renault for helpful discussion. This work was supported by the Department of Defense, Defense Threat Reduction Agency (Contract HDTRA1-11-1-0005). J.E.D. was supported by a National Science Foundation Graduate Research Fellowship under Grant DGE-1110007. Work in the Upton laboratory is supported by the Cancer Prevention & Research Institute of Texas under Scholar Award R1202.

1. Xiao X, Bard AJ (2007) Observing single nanoparticle collisions at an ultramicroelectrode by electrocatalytic amplification. *J Am Chem Soc* 129(31):9610–9612.
2. Zhou Y-G, Rees NV, Compton RG (2011) The electrochemical detection and characterization of silver nanoparticles in aqueous solution. *Angew Chem Int Ed Engl* 50(18):4219–4221.
3. Zhou H, Fan F-RF, Bard AJ (2010) Observation of discrete Au nanoparticle collisions by electrocatalytic amplification using Pt ultramicroelectrode surface modification. *J Phys Chem Lett* 1:2671–2674.
4. Zhou Y-G, Haddou B, Rees NV, Compton RG (2012) The charge transfer kinetics of the oxidation of silver and nickel nanoparticles via particle-electrode impact electrochemistry. *Phys Chem Chem Phys* 14(41):14354–14357.
5. Haddou B, Rees NV, Compton RG (2012) Nanoparticle-electrode impacts: The oxidation of copper nanoparticles has slow kinetics. *Phys Chem Chem Phys* 14(39):13612–13617.
6. Kwon SJ, Fan F-RF, Bard AJ (2010) Observing iridium oxide (IrO(x)) single nanoparticle collisions at ultramicroelectrodes. *J Am Chem Soc* 132(38):13165–13167.
7. Sardesai NP, Andreescu D, Andreescu S (2013) Electroanalytical evaluation of antioxidant activity of cerium oxide nanoparticles by nanoparticle collisions at microelectrodes. *J Am Chem Soc* 135(45):16770–16773.
8. Fernando A, Parajuli S, Alpuche-Aviles MA (2013) Observation of individual semiconducting nanoparticle collisions by stochastic photoelectrochemical currents. *J Am Chem Soc* 135(30):10894–10897.
9. Boika A, Thorgaard SN, Bard AJ (2013) Monitoring the electrophoretic migration and adsorption of single insulating nanoparticles at ultramicroelectrodes. *J Phys Chem B* 117(16):4371–4380.
10. Cheng W, Zhou XF, Compton RG (2013) Electrochemical sizing of organic nanoparticles. *Angew Chem Int Ed Engl* 52(49):12980–12982.
11. Quinn BM, Van 't Hof PG, Lemay SG (2004) Time-resolved electrochemical detection of discrete adsorption events. *J Am Chem Soc* 126(27):8360–8361.
12. Stuart EJE, Tschulik K, Batchelor-McAuley C, Compton RG (2014) Electrochemical observation of single collision events: Fullerene nanoparticles. *ACS Nano* 8(8):7648–7654.
13. Kim B-K, Boika A, Kim J, Dick JE, Bard AJ (2014) Characterizing emulsions by observation of single droplet collisions—attoliter electrochemical reactors. *J Am Chem Soc* 136(13):4849–4852.
14. Cheng W, Compton RG (2014) Investigation of single-drug-encapsulating liposomes using the nano-impact method. *Angew Chem Int Ed Engl* 53(50):13928–13930.
15. Dick JE, Renault C, Kim B-K, Bard AJ (2014) Simultaneous detection of single attoliter droplet collisions by electrochemical and electrogenerated chemiluminescent responses. *Angew Chem Int Ed Engl* 53(44):11859–11862.
16. Zhou H, Park JH, Fan F-RF, Bard AJ (2012) Observation of single metal nanoparticle collisions by open circuit (mixed) potential changes at an ultramicroelectrode. *J Am Chem Soc* 134(32):13212–13215.
17. Dick JE, Renault C, Kim BK, Bard AJ (2014) Electrogenerated chemiluminescence of common organic luminophores in water using an emulsion system. *J Am Chem Soc* 136(39):13546–13549.
18. Fan F-RF, Bard AJ (2008) Observing single nanoparticle collisions by electrogenerated chemiluminescence amplification. *Nano Lett* 8(6):1746–1749.
19. Kolthoff IM, Tomsicek WJ (1935) The oxidation potential of the system potassium ferrocyanide-potassium ferricyanide at various ionic strengths. *J Phys Chem* 39:945–954.
20. Davies CW (1937) The conductance of potassium ferrocyanide solutions. *J Am Chem Soc* 59:1760–1761.
21. Panckhurst MH, Woolmington KG (1957) A spectrophotometric study of ionic association in aqueous solutions. *Proc R Soc Lond* 244(9):124–139.
22. James JC (1949) The conductivities of dilute aqueous solutions of potassium ferrocyanide and calcium ferrocyanide. *Trans Faraday Soc* 45:855–861.
23. Kwon SJ, Bard AJ (2012) DNA analysis by application of Pt nanoparticle electrochemical amplification with single label response. *J Am Chem Soc* 134(26):10777–10779.
24. Griffiths P, Baraniak I, Reeves M (2015) The pathogenesis of human cytomegalovirus. *J Pathol* 235(2):288–297.
25. Dollard SC, Grosse SD, Ross DS (2007) New estimates of the prevalence of neurological and sensory sequelae and mortality associated with congenital cytomegalovirus infection. *Rev Med Virol* 17(5):355–363.
26. Ellison J, et al. (2013) Get more out of your data: A new approach to agglomeration and aggregation studies using nanoparticle impact experiments. *ChemistryOpen* 2(2):69–75.
27. Fosdick SE, Anderson MJ, Nettleton EG, Crooks RM (2013) Correlated electrochemical and optical tracking of discrete collision events. *J Am Chem Soc* 135(16):5994–5997.
28. Kwon SJ, et al. (2011) Stochastic electrochemistry with electrocatalytic nanoparticles at inert ultramicroelectrodes—theory and experiments. *Phys Chem Chem Phys* 13(12):5394–5402.
29. Einstein A (1905) Über die von der molekularkinetischen Theorie der Wärme geforderte Bewegung von in ruhenden Flüssigkeiten suspendierten Teilchen. *Annr Phys* 322:549–560.
30. Heldwein EE, Krummenacher C (2008) Entry of herpesviruses into mammalian cells. *Cell Mol Life Sci* 65(11):1653–1668.
31. Cekinović D, et al. (2008) Passive immunization reduces murine cytomegalovirus-induced brain pathology in newborn mice. *J Virol* 82(24):12172–12180.
32. Tan YH, et al. (2008) A nanoengineering approach for investigation and regulation of protein immobilization. *ACS Nano* 2(11):2374–2384.
33. Mirkin CA, Letsinger RL, Mucic RC, Storhoff JJ (1996) A DNA-based method for rationally assembling nanoparticles into macroscopic materials. *Nature* 382(6592):607–609.
34. Mucic RC, Storhoff JJ, Mirkin CA, Letsinger RL (1998) DNA-directed synthesis of binary nanoparticle network materials. *J Am Chem Soc* 120:12674–12675.
35. Hui JP, Boika A, Park HS, Lee HC, Bard AJ (2013) Single collision events of conductive nanoparticles driven by migration. *J Phys Chem C* 117:6651–6657.
36. Yoo JJ, Anderson MJ, Alligrant TM, Crooks RM (2014) Electrochemical detection of insulating beads at subattomolar concentration via magnetic enrichment in a microfluidic device. *Anal Chem* 86(9):4302–4307.
37. Bard AJ (2004) *Electrogenerated Chemiluminescence* (Marcel Dekker, New York).
38. Fan F-RF, Demaille C (2001) The preparation of tips for scanning electrochemical microscopy. *Scanning Electrochemical Microscopy*, eds Mirkin MV, Bard AJ (Marcel Dekker, New York), 2nd Ed, pp 75–78.
39. Redwood AJ, et al. (2005) Use of a murine cytomegalovirus K181-derived bacterial artificial chromosome as a vaccine vector for immunocontraception. *J Virol* 79(5):2998–3008.
40. Clambey ET, Virgin HW, 4th, Speck SH (2000) Disruption of the murine gammaherpesvirus 68 M1 open reading frame leads to enhanced reactivation from latency. *J Virol* 74(4):1973–1984.
41. Saederup N, Lin YC, Dairaghi DJ, Schall TJ, Mocarski ES (1999) Cytomegalovirus-encoded beta chemokine promotes monocyte-associated viremia in the host. *Proc Natl Acad Sci USA* 96(19):10881–10886.
42. Britt WJ (2010) Human cytomegalovirus: Propagation, quantification, and storage. *Current Protocols in Microbiology*, eds McBride A, Quarles JM, Stevenson B, Taylor RK (Wiley, New York), p 14E3.